

# RSC Advances



This is an *Accepted Manuscript*, which has been through the Royal Society of Chemistry peer review process and has been accepted for publication.

*Accepted Manuscripts* are published online shortly after acceptance, before technical editing, formatting and proof reading. Using this free service, authors can make their results available to the community, in citable form, before we publish the edited article. This *Accepted Manuscript* will be replaced by the edited, formatted and paginated article as soon as this is available.

You can find more information about *Accepted Manuscripts* in the [Information for Authors](#).

Please note that technical editing may introduce minor changes to the text and/or graphics, which may alter content. The journal's standard [Terms & Conditions](#) and the [Ethical guidelines](#) still apply. In no event shall the Royal Society of Chemistry be held responsible for any errors or omissions in this *Accepted Manuscript* or any consequences arising from the use of any information it contains.

# Toward elevated light harvesting: Efficient dye-sensitized solar cells with titanium dioxide/silica photoanodes

Peizhi Yang<sup>1\*</sup>, Qunwei Tang<sup>2\*</sup>, Benlin He<sup>2</sup>

<sup>1</sup> Key Laboratory of Advanced Technique & Preparation for Renewable Energy Materials, Ministry of Education, Yunnan Normal University, Kunming 650092, PR China;

<sup>2</sup> Institute of Materials Science and Engineering, Ocean University of China, Qingdao 266100, PR China;

E-mail address: pzhyang@hotmail.com; tangqunwei@ouc.edu.cn; Tel/Fax: 86 532 66782533;

**Abstract:** Pursuit of light harvesting is a persistent objective for dye-sensitized solar cells (DSSCs). Here we report the synthesis of titanium dioxide/silica (TiO<sub>2</sub>/SiO<sub>2</sub>) nanocrystallite photoanodes, aiming at elevating the light harvesting for dye excitation. Due to light interference effect of the reflected light beams from TiO<sub>2</sub>/SiO<sub>2</sub> and SiO<sub>2</sub>/electrolyte interfaces, the dye excitation and therefore the photocurrent density are markedly enhanced. The photovoltaic performances of the resultant DSSCs are optimized by utilizing three TiO<sub>2</sub>/SiO<sub>2</sub> photoanodes from different synthesis strategies. A maximum power conversion efficiency of 8.56% is measured under simulated air mass 1.5 global sunlight in comparison with 7.06% from pristine TiO<sub>2</sub> based DSSC. The high power conversion efficiency in combination with simple preparation demonstrates the potential utilization of TiO<sub>2</sub>/SiO<sub>2</sub> nanocrystallite anodes for efficient DSSCs.

## 1. Introduction

The depletion of fossil fuels and global warming pose a challenge against the sustainable

development of the world. One of the efficient solutions is to explore renewable energy resources. Solar energy accounts for 99% of earth energy, therefore the direct conversion of solar energy into electricity has attracted widespread attention due to low environmental impacts.<sup>1-3</sup> Dye-sensitized solar cell (DSSC), a photoelectrochemical device comprising of a dye-sensitized anode, a redox electrolyte having  $I^-/I_3^-$  couples, and a counter electrode, has attracted growing interests because of its merits on cost-effectiveness, relatively high power conversion efficiency, easy fabrication, and environmental friendliness.<sup>4-8</sup> Since the first DSSC prototype created by Grätzel in 1991,<sup>9</sup> the maximum efficiency of ~13% has been recorded under simulated air mass 1.5 (AM1.5) global sunlight.<sup>10</sup> One of the main problems in restricting the enhancement in power conversion efficiency is the incompleting dye excitation, therefore resulting in a modest electron density on conduction band (CB) of  $TiO_2$  anode.<sup>11</sup> Many efforts have been made to enhance the dye excitation, such as building reflecting layer<sup>12,13</sup> and designing bifacial DSSC that can be simultaneously illuminated from both front and rear sides.<sup>14</sup> Recently, a bifacial DSSC device has been successfully designed in our group by splitting incident light into two beams.<sup>14</sup> The device is simultaneously irradiated from  $TiO_2$  photoanode and transparent polyaniline counter electrode. The incident light from transparent polyaniline counter electrode can compensate for the light penetrated from photoanode, leading to a significantly enhanced dye excitation and a promising power conversion efficiency of 8.35%.

In searching for other alternative strategies, here we launch three hydrothermal methods for the design of  $TiO_2/SiO_2$  anodes in an attempt to increase the electron density on CB of  $TiO_2$  nanocrystallites. The light intensity for dye excitation is expected to be markedly enhanced due to the interference light reflected from  $TiO_2/SiO_2$  and  $SiO_2/air$  (electrolyte) interfaces. The concept toward light harvesting is also significant for other solar cells, such as quantum dot-sensitized solar cells, perovskite solar cells.

## 2. Experimental

### 2.1. Materials

Unless noted otherwise, all the chemicals were purchased from Sigma–Aldrich and used as received. The average diameter of commercial SiO<sub>2</sub> nanoparticles is around 20 nm.

### 2.2. Preparation of TiO<sub>2</sub>/SiO<sub>2</sub> nanocrystallites

The TiO<sub>2</sub>/SiO<sub>2</sub> nanocrystallites can be prepared according to the following procedures: (1) Under vigorous agitation at room temperature, 100 mL of deionized water was mixed with 10 mL of titanium tetrabutanolate. After 30 min, the mixture was pump–filtrated to obtain dehydrated filter powders. (2) Subsequently, 10 mL of acetic acid and 0.8 mL of nitric acid were added into the above filter powders dropwise in a flask. After an agitation of 15 min at 80 °C, the volume of the mixture was adjusted to 170 mL by adding deionized water. The reactant was further agitated at 80 °C in a sealed atmosphere. (3) Later, the resultant colloid was transferred into a Teflon–lined autoclave and heated at 200 °C for 12 h. (4) A homogeneous mixture consisting of 65 mL of the white colloid and 0.4 g of commercial P25 were made under ultrasonic irradiation for 30 min and (5) then transferred to another Teflon–lined autoclave, which was subsequently heated at 200 °C for 12 h. (6) After removing supernatant liquid, the colloid was mixed with 0.8 g of poly(ethylene glycol) ( $M_w = 20,000$ ) and 1 mL of OP emulsifier and subsequently concentrated at 80 °C. To obtain the TiO<sub>2</sub>/SiO<sub>2</sub> colloid, 0.0275 g of SiO<sub>2</sub> nanoparticles were added into above reagent after steps (2), (4), and (6), the as–synthesized samples were denoted as TiO<sub>2</sub>/SiO<sub>2</sub>–(i), TiO<sub>2</sub>/SiO<sub>2</sub>–(ii), and TiO<sub>2</sub>/SiO<sub>2</sub>–(iii), respectively.

### 2.3. Fabrication of photoanodes

Fluorine doped tin oxide (FTO) glass substrates (sheet resistance: 12 Ω square<sup>-1</sup>) with a size of 2 × 2

cm<sup>2</sup> were thoroughly rinsed by deionized water and anhydrous ethanol, and dried by N<sub>2</sub> gas flow. The photoanodes from TiO<sub>2</sub>/SiO<sub>2</sub> were fabricated by a screen printing technique. The size of the resultant photoanodes was controlled at 0.5 × 0.5 cm<sup>2</sup> with an average thickness of TiO<sub>2</sub>/SiO<sub>2</sub> layer of 10 μm. The air-dried colloids were calcined in a muffle furnace at 450 °C for 30 min. The elevation of heating temperature was controlled at a speed of 2 °C min<sup>-1</sup> till 130 °C, and then at a speed of 6 °C min<sup>-1</sup> until 450 °C. The resultant TiO<sub>2</sub>/SiO<sub>2</sub> films were immersed in 0.50 mM N719 ethanol solution for 24 h to obtain dye-sensitized TiO<sub>2</sub>/SiO<sub>2</sub> photoanodes.

#### 2.4. Assembly of DSSCs

Each DSSC was assembled by sandwiching a dye-sensitized TiO<sub>2</sub>/SiO<sub>2</sub> photoanode, a liquid electrolyte having I<sup>-</sup>/I<sub>3</sub><sup>-</sup> redox couples, and a Pt counter electrode. A redox electrolyte consisted of 100 mM of tetraethylammonium iodide, 100 mM of tetramethylammonium iodide, 100 mM of tetrabutylammonium iodide, 100 mM of NaI, 100 mM of KI, 100 mM of LiI, 50 mM of I<sub>2</sub>, and 500 mM of 4-tert-butyl-pyridine in 50 ml acetonitrile. The photocurrent-voltage (*J-V*) curves of the assembled DSSCs were recorded on an Electrochemical Workstation (CHI600E) under irradiation of a simulated solar light (Xe Lamp Oriel Sol<sup>3</sup>A™ Class AAA Solar Simulators 94023A, USA) at a light intensity of 100 mW cm<sup>-2</sup> (calibrated by a standard silicon solar cell) in ambient atmosphere. A black mask with an aperture area of around 0.25 cm<sup>2</sup> was applied on the surface of DSSCs to avoid stray light. Each DSSC device was measured at least five times to eliminate experimental error (± 5%) and a compromise *J-V* curve was employed.

#### 2.5. Other characterizations

The morphologies of the resultant TiO<sub>2</sub>/SiO<sub>2</sub> and pure TiO<sub>2</sub> anodes were observed with a scanning electron microscope (SEM, S-3500N, Hitachi, Japan) and a transmission electron microscopy (TEM, JEM2010, JEOL). The optical absorption spectra were recorded on a UV-vis

spectrophotometer (Agilent 8453) at room temperature. Fourier transformed Raman spectroscopic measurements in the ultraviolet light were performed on a Renishaw inVia Reflex Raman Spectrometer. High-resolution gratings were used to give a spectral resolution of  $2\text{ cm}^{-1}$ . The spectra were recorded at room temperature from  $3200$  to  $100\text{ cm}^{-1}$  using 16 scans with an exposure time of 1 s per scan. X-ray diffraction (XRD) profiles of the resultant nanocrystallites were recorded on an X-ray powder diffractometer (X'pert MPD Pro, Philips, Netherlands) with  $\text{Cu K}\alpha$  radiation ( $\lambda = 1.542\text{ \AA}$ ) in the  $2\theta$  range from  $10$  to  $70^\circ$  operating at  $40\text{ kV}$  accelerating voltage and  $40\text{ mA}$  current). Fourier transform infrared spectrometry (FTIR) spectra were recorded on a Vertex 70 FTIR spectrometer (Bruker). For electrochemical impedance spectroscopy (EIS) measurements, the DSSCs were scanned from  $0.1\text{ Hz}$  to  $1\text{ MHz}$  at an ac amplitude of  $10\text{ mV}$ .

### 3. Results and discussion

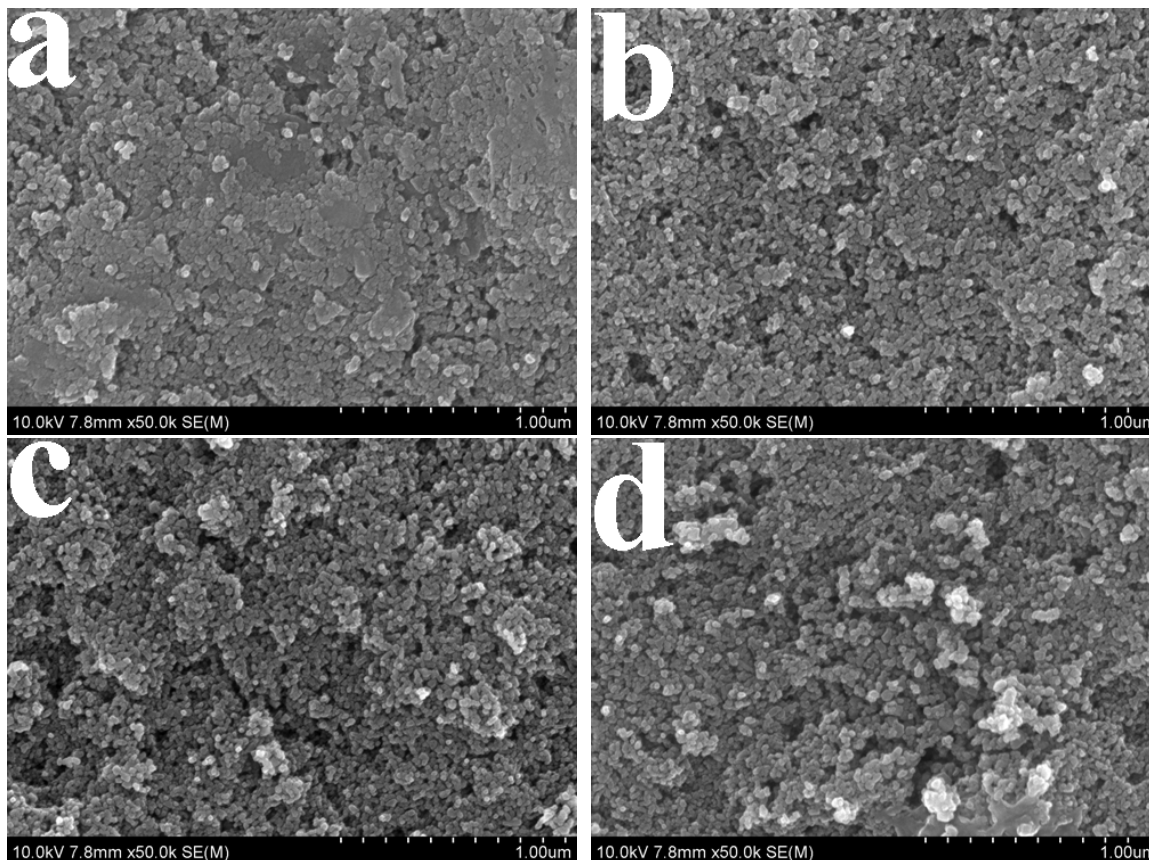


**Fig. 1** SEM photographs of the TiO<sub>2</sub>/SiO<sub>2</sub> and pure TiO<sub>2</sub> nanocrystallites: (a) TiO<sub>2</sub>/SiO<sub>2</sub>–(i), (b) TiO<sub>2</sub>/SiO<sub>2</sub>–(ii), (c) TiO<sub>2</sub>/SiO<sub>2</sub>–(iii), and (d) pure TiO<sub>2</sub>.

The morphology of a TiO<sub>2</sub> nanocrystallite photoanode is crucial for DSSC device.<sup>15</sup> Here, we mainly describe the morphological difference of resultant TiO<sub>2</sub>/SiO<sub>2</sub> and pure TiO<sub>2</sub> prepared by the sol–hydrothermal method. As is shown in Fig. 1, no apparent deviations in morphologies are observed from SEM images, indicating that the synthesis strategy does not have influences on the morphology of resultant TiO<sub>2</sub>/SiO<sub>2</sub> anodes. The BET surface areas of the samples are 46.2, 62.0, 96.7, and 73.5 m<sup>2</sup> g<sup>-1</sup> for pure TiO<sub>2</sub>, TiO<sub>2</sub>/SiO<sub>2</sub>–(i), TiO<sub>2</sub>/SiO<sub>2</sub>–(ii), and TiO<sub>2</sub>/SiO<sub>2</sub>–(iii), respectively. The task of a photoanode is to adsorb dyes and to transfer photogenerated electrons from excited dye to FTO layer along the percolating networks of TiO<sub>2</sub>, therefore the mesoporous structure having high specific surface area demonstrates it is feasible to upload more photosensitive dyes for electron generation. As a reference, the surface morphology of pristine TiO<sub>2</sub> anode is also provided, giving no apparent difference from TiO<sub>2</sub>/SiO<sub>2</sub>–(ii). Moreover, we can not distinguish SiO<sub>2</sub> from TiO<sub>2</sub> nanoparticles in SEM photographs, or amorphous SiO<sub>2</sub> nanoparticles maybe suffer from dissolution and reorganization during the rigorous hydrothermal conditions.

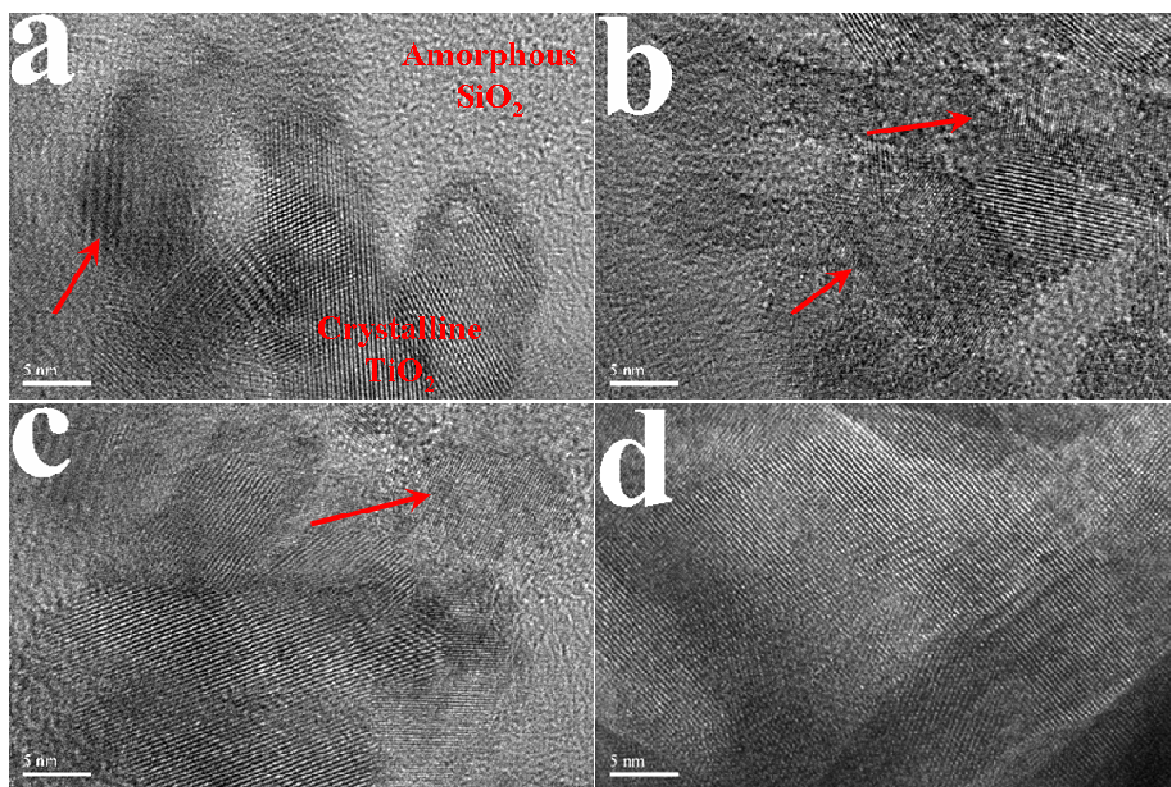


**Fig. 2** TEM photographs of the  $\text{TiO}_2/\text{SiO}_2$  and pure  $\text{TiO}_2$  nanocrystallites: (a)  $\text{TiO}_2/\text{SiO}_2$ -(i), (b)  $\text{TiO}_2/\text{SiO}_2$ -(ii), (c)  $\text{TiO}_2/\text{SiO}_2$ -(iii), and (d) pure  $\text{TiO}_2$ . The distortions and defects have been marked in the figures.

Fig. 2 displays the high-resolution TEM images of  $\text{TiO}_2/\text{SiO}_2$  and pure  $\text{TiO}_2$  nanocrystallites. It can be seen that the crystal lattice of the pure  $\text{TiO}_2$  is homogeneous with no amorphous regions, indicating that the organics and carbonaceous materials have been removed during calcination process. However, a great deal of lattice distortions and plenty of defects are detected in the three  $\text{TiO}_2/\text{SiO}_2$  nanocrystallites. Due to fact of amorphous phase of  $\text{SiO}_2$ , we deduce the amorphous regions refer to  $\text{SiO}_2$  phase and the crystal phase means anatase  $\text{TiO}_2$ . These results reveal that  $\text{TiO}_2$  has been successfully incorporated or partially incorporated with amorphous  $\text{SiO}_2$  by entering the lattice fringes of  $\text{TiO}_2$  by  $\text{Si}^{4+}$  ions.<sup>16</sup> It has been known that the ionic radii of  $\text{Si}^{4+}$  (0.039 nm) is much smaller than that of  $\text{Ti}^{4+}$  (0.068 nm), suggesting that  $\text{Si}^{4+}$  ions can enter into  $\text{TiO}_2$  crystal lattice to substitute for  $\text{Ti}^{4+}$ , which is consistent with the morphology analysis.

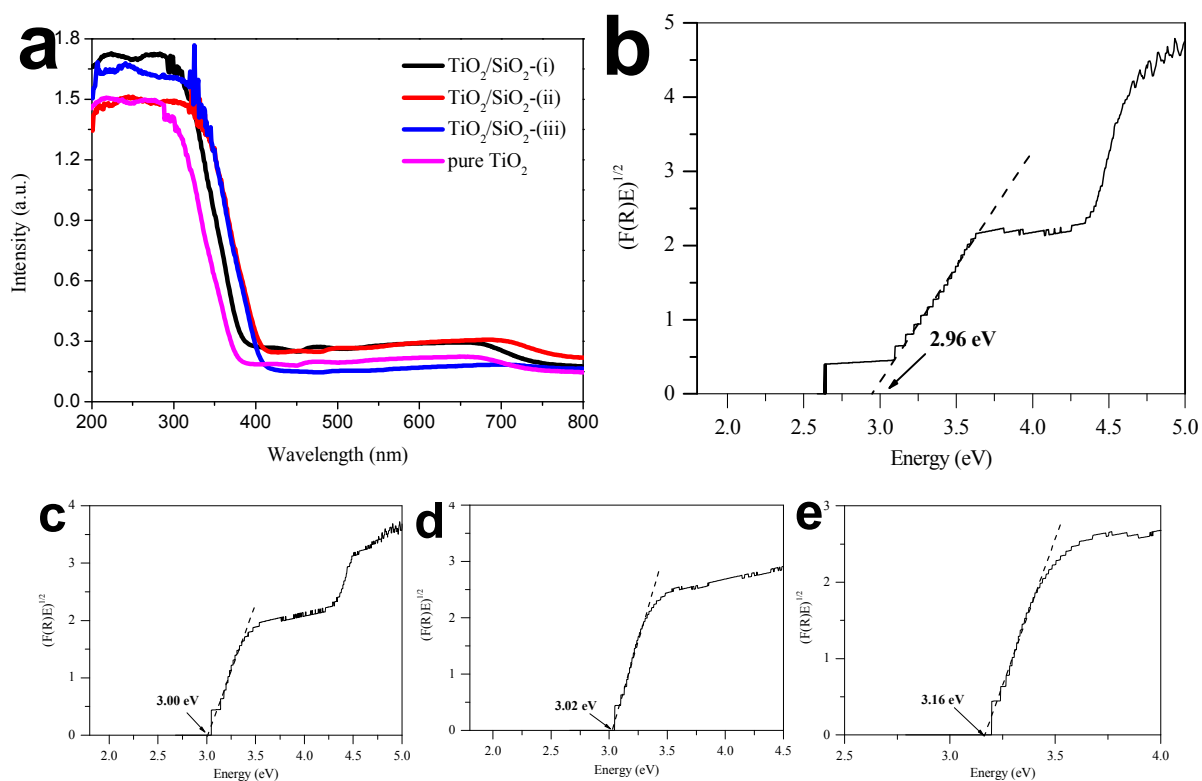


**Fig. 3** (a) UV–vis diffuse reflection spectra of the  $\text{TiO}_2/\text{SiO}_2$  and pure  $\text{TiO}_2$  nanocrystallites. Plots of  $(F(R_\infty)E)^{1/2}$  as a function of energy for (b) pristine  $\text{TiO}_2$ , (c)  $\text{TiO}_2/\text{SiO}_2$ -(i), (d)  $\text{TiO}_2/\text{SiO}_2$ -(ii), and (e)  $\text{TiO}_2/\text{SiO}_2$ -(iii).

In order to describe the photo-absorption behavior of the  $\text{TiO}_2/\text{SiO}_2$  nanocrystallites, the UV–vis diffuse reflection spectra have been recorded and shown in Fig. 3. As a comparison, the absorption spectrum of the pristine  $\text{TiO}_2$  is also conducted at the same conditions. No obvious shape alteration is observed after being integrated by  $\text{SiO}_2$ . Pristine  $\text{TiO}_2$  exhibits an absorption band at ca. 396 nm. However, the absorption shifts towards ultraviolet–light region. Reflectance spectra have been converted to the absorbance spectra using Kubelka–Munk equations (Eqs 1&2).<sup>17</sup>

$$F(R_\infty(\lambda)) = \frac{(1 - R_\infty)^2}{2R_\infty} \quad (1)$$

$$R_\infty = \frac{R}{R_{\text{BaSO}_4}} \quad (2)$$

where  $R$  is the reflectance recorded for a sample and  $R_{\text{BaSO}_4}$  is the reflectance recorder for a reference. To calculate the band-gap energy, the Kubelka–Munk function is converted to the form

$(F(R_\infty)E)^{1/2}$  and the wavelength is changed to energy units (eV). The direct band gap energy can be recorded by an extrapolation method (see Fig. 3b-e). The direct  $E_g$  values of pure  $\text{TiO}_2$ ,  $\text{TiO}_2/\text{SiO}_2$ -(i),  $\text{TiO}_2/\text{SiO}_2$ -(ii), and  $\text{TiO}_2/\text{SiO}_2$ -(iii) are 2.96, 3.00, 3.02, and 3.16 eV, respectively. Notably,  $\text{TiO}_2$  is a typical photocatalyst and has been utilized for dye removal from pollutions.<sup>18-20</sup> When irradiated by incident light, the electrons on valence band of  $\text{TiO}_2$  can absorb energy and jump to its conduction band, leaving holes to  $\text{TiO}_2$  surface. Both photogenerated electrons and holes by  $\text{TiO}_2$  can participate in the degradation reactions of organic dyes. In this fashion, the N719 molecule, one of the organic dyes, is expected to be photodegraded by  $\text{TiO}_2$ , while the wavelength of the light for dye degradation depends on the  $E_g$  of the  $\text{TiO}_2$  ( $E_g \approx 1240/\lambda$ ). Apparently, the as-synthesized  $\text{TiO}_2/\text{SiO}_2$ -(ii) has the highest  $E_g$ , which indicates the excitation of photogenerated electrons and holes requires increased photon energy. Therefore, less electron-hole pairs can be produced in the  $\text{TiO}_2/\text{SiO}_2$ -(ii) for participating the photodegradation of organic N719 dye molecules, leading to an enhanced dye stability by utilizing strategy (ii) for photoanode fabrication.

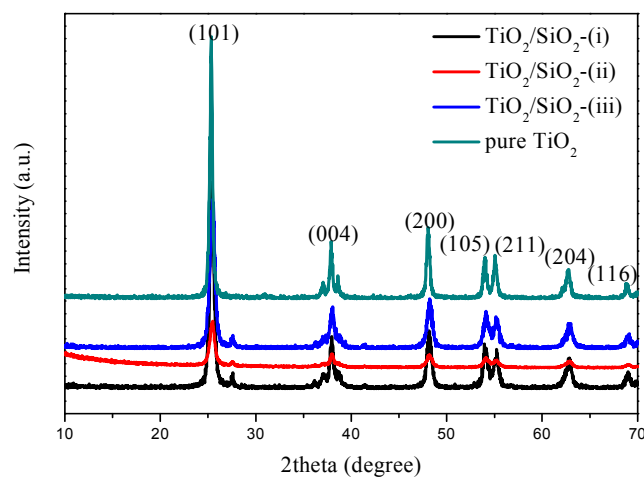


**Fig. 4** XRD patterns of the  $\text{TiO}_2/\text{SiO}_2$  and pure  $\text{TiO}_2$  nanocrystallites.

**Table 1** Structure parameters obtained from XRD patterns of pure  $\text{TiO}_2$  and  $\text{TiO}_2/\text{SiO}_2$  nanocrystallites.

Nanocrystallites	$\beta$ ( $^\circ$ )	$2\theta$ ( $^\circ$ )	Crystallite size (nm)	$\Delta d/d$
------------------	----------------------	------------------------	-----------------------	--------------

pure TiO <sub>2</sub>	0.32	25.45	25.19	0.00752
TiO <sub>2</sub> /SiO <sub>2</sub> -(i)	0.48	25.45	16.66	0.0113
TiO <sub>2</sub> /SiO <sub>2</sub> -(ii)	0.58	25.45	13.79	0.0136
TiO <sub>2</sub> /SiO <sub>2</sub> -(iii)	0.56	25.45	14.28	0.0132

XRD technique has been widely employed for the identification of crystal phase as well as crystallite size of TiO<sub>2</sub>. The detection of diffraction peaks reveals that the pristine TiO<sub>2</sub> is featured by anatase phase (Fig. 4). No diffraction peaks of rutile phase are detected in the XRD patterns. The crystallite size can be determined from the broadening of corresponding XRD peaks by Scherrer formula:<sup>21</sup>

$$L = \frac{K\lambda}{\beta \cos \theta} \quad (3)$$

where  $L$  is the crystallite size,  $\lambda$  is the wavelength of the X-ray radiation ( $\text{CuK}\alpha = 0.15418 \text{ nm}$ ),  $K$  is usually taken as 0.89, and  $\beta$  is the line width at half-maximum height (FWHM). In addition, the crystal lattice distortion ( $\Delta d/d$ ) can also be evaluated from the equation:<sup>22</sup>

$$\frac{\Delta d}{d} = \frac{\beta}{4 \tan \theta} \quad (4)$$

At the first glance, all the diffraction peaks belonging to the diffraction faces of anatase TiO<sub>2</sub> can be detected in the TiO<sub>2</sub>/SiO<sub>2</sub> nanocrystallites. However, the relative intensity of diffraction peak belonging to (101) face of anatase TiO<sub>2</sub> phase dramatically decreases after being doped by Si<sup>4+</sup>, indicating an inhibition effect of phase transformation from amorphous to anatase TiO<sub>2</sub>. Moreover, the crystallite size of the TiO<sub>2</sub>/SiO<sub>2</sub> has an order of decreasing and the TiO<sub>2</sub>/SiO<sub>2</sub>-(ii) has the smallest crystallite size (Table 1), suggesting that the doping of Si<sup>4+</sup> in TiO<sub>2</sub> can hinder the growth of crystallite size due to the segregation of dopant cations at the grain boundary.<sup>23</sup> The crystal lattice distortion ( $\Delta d/d$ ) is also elevated by doping Si<sup>4+</sup> ions in comparison with that of pure TiO<sub>2</sub>, indicating that the substitution of Ti by Si can generate more defects for dye adsorption. This result is in an agreement with TEM observation.

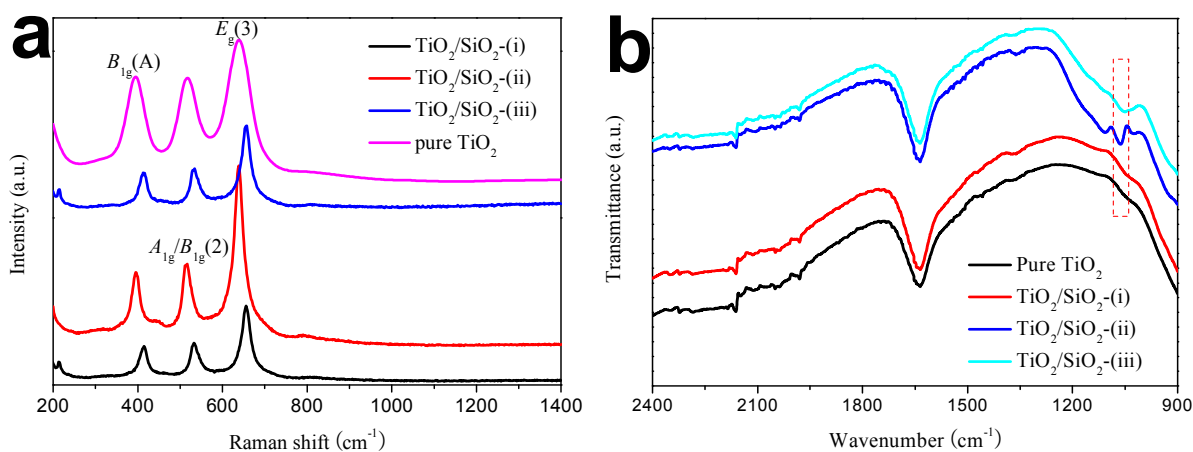


**Fig. 5** (a) Raman and (b) FTIR spectra of  $\text{TiO}_2/\text{SiO}_2$  and pure  $\text{TiO}_2$  nanocrystallites.

Crystallographic structures of the  $\text{TiO}_2/\text{SiO}_2$  and pure  $\text{TiO}_2$  nanocrystallites are judged by Raman spectroscopy and shown in Fig. 5a. The whole set of spectra shows three main Raman peaks at 394, 515, and 639  $\text{cm}^{-1}$  that can be ascribed to the  $B_{1g}(1)$ ,  $A_{1g}/B_{1g}(2)$ , and  $E_g(3)$  modes of anatase phase of pure  $\text{TiO}_2$ , respectively. However, the mode positions have shifted in comparison with pure  $\text{TiO}_2$ . It is attributed to the decrease in crystallite size (Table 1) and lack of adjacent atoms for the surface atoms. Therefore, the surface atoms are in a relaxation state and the red shift results from a surface relaxation effect.<sup>24</sup> Although the positions have deviations, the doping of  $\text{Si}^{4+}$  does not influence and change the structure of  $\text{TiO}_2$ .<sup>25</sup> The conclusion is consistent with that of XRD analysis. No Raman peaks corresponding to  $\text{SiO}_2$  can be detected in the doped  $\text{TiO}_2$ , indicating that  $\text{Si}^{4+}$  may present in the substitutional positions in the crystal lattice of  $\text{TiO}_2$ . The detection of 1059  $\text{cm}^{-1}$  in FTIR spectra (Fig. 5b) is a signal of Si–O–Ti bond,<sup>26,27</sup> indicating that there is a covalent bond between  $\text{SiO}_2$  and  $\text{TiO}_2$  instead of a simple mixture. The coverage of  $\text{TiO}_2$  by  $\text{SiO}_2$  layer along with the doping of  $\text{TiO}_2$  by  $\text{SiO}_2$  and detection of Si–O–Ti bond may be used to support the hypothesis that the amorphous  $\text{SiO}_2$  nanoparticles have been dissolved and reorganized in the hydrothermal process.

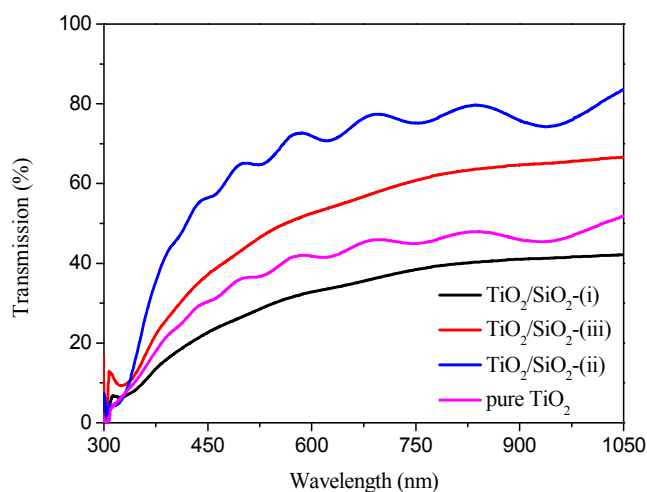


**Fig. 6** Transmission spectra of TiO<sub>2</sub>/SiO<sub>2</sub> and pure TiO<sub>2</sub> nanocrystallites.

Incident light intensity of  $100 \text{ mW cm}^{-2}$  (AM1.5G) has been widely employed as a standard in evaluating the DSSC performances. In our previous study,<sup>11</sup> we found that  $\sim 85$  and  $\sim 40 \text{ mW cm}^{-2}$  of incident light is remained after penetrating FTO glass and  $10 \mu\text{m}$ -thickness FTO-TiO<sub>2</sub> photoanode (Fig. 6), respectively. This indicates that the dye molecules adsorbed at the interface of TiO<sub>2</sub>/FTO are irradiated by incident light with an intensity of  $\sim 85 \text{ mW cm}^{-2}$ , whereas it is  $\sim 40 \text{ mW cm}^{-2}$  for the dyes at the interface of TiO<sub>2</sub>/electrolyte. The incident light has trend of a gradient descent within dye-sensitized TiO<sub>2</sub> film because of reflection and absorption of TiO<sub>2</sub> nanocrystallites. It is well known that the DSSC performances are highly dependent on incident light intensity.<sup>28-30</sup> Therefore, the transmission enhancement is of great significance in improving the photovoltaic performances. Interestingly, the transmission is dramatically enhanced by synthesizing TiO<sub>2</sub>/SiO<sub>2</sub> by route (ii), it is  $\sim 80 \text{ mW cm}^{-2}$  in light intensity across the  $10 \mu\text{m}$ -thickness FTO-TiO<sub>2</sub>/SiO<sub>2</sub> anode. To explore the potential mechanism, we think it subjects to the compensation effect of reflected light from TiO<sub>2</sub>/SiO<sub>2</sub> and SiO<sub>2</sub>/electrolyte interfaces. The transmission enhancement is attributed to a good matching of  $\sqrt{n_{\text{TiO}_2}}$  with  $n_{\text{SiO}_2}$  (Supporting Information).<sup>11</sup> Until now, we can make a conclusion that the dye excitation efficiency is expected to be significantly enhanced, which is contributive to the elevation of electron density on CB of TiO<sub>2</sub> and therefore the photocurrent density of the DSSC.

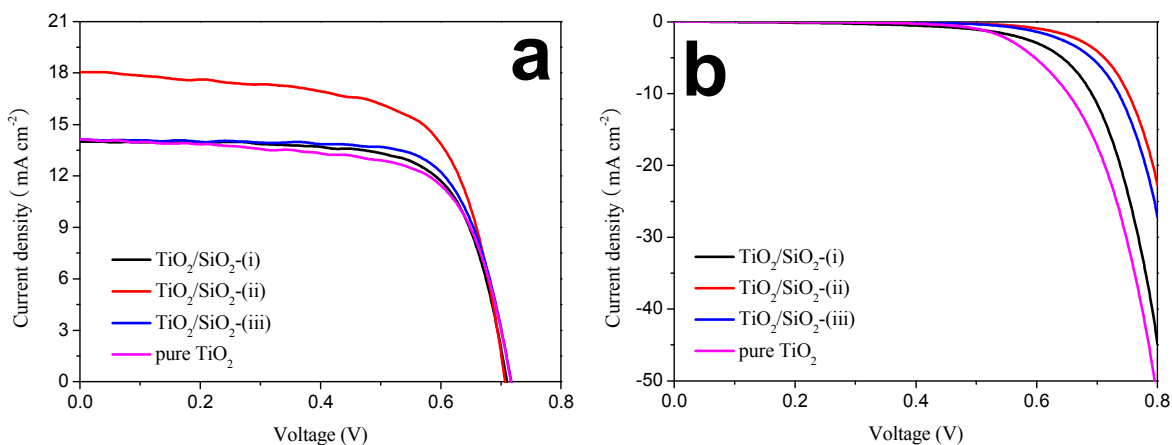


**Fig. 7**  $J$ - $V$  characteristics of DSSCs from various nanocrystallite anodes: (a) illuminated under AM1.5 and (b) in the dark.

**Table 2** Photovoltaic parameters of the DSSCs using various nanocrystallite anodes.  $J_{sc}$ : short-circuit current density;  $V_{oc}$ : open-circuit voltage,  $FF$ : fill factor;  $PCE$ : power conversion efficiency.

DSSCs	$V_{oc}$ (V)	$J_{sc}$ (mA cm <sup>-2</sup> )	$FF$	PCE (%)
TiO <sub>2</sub> /SiO <sub>2</sub> -(i)	0.710	14.13	0.73	7.30
TiO <sub>2</sub> /SiO <sub>2</sub> -(ii)	0.708	18.06	0.65	8.56
TiO <sub>2</sub> /SiO <sub>2</sub> -(iii)	0.770	14.10	0.69	7.52
Pure TiO <sub>2</sub>	0.718	14.06	0.70	7.06

Fig. 7a displays  $J$ - $V$  curves of the DSSCs from TiO<sub>2</sub>/SiO<sub>2</sub> and pure TiO<sub>2</sub> photoanodes and the photovoltaic parameters are summarized in Table 2. The DSSC device containing pure TiO<sub>2</sub> crystallites gives a  $J_{sc}$  of 14.06 mA cm<sup>-2</sup> and  $\eta$  of 7.06%. Both of these parameters are enhanced by employing TiO<sub>2</sub>/SiO<sub>2</sub> anodes. The optimal photovoltaic performances result from TiO<sub>2</sub>/SiO<sub>2</sub>-(ii) based DSSC:  $J_{sc}$  of 18.06 mA cm<sup>-2</sup> and  $\eta$  of 8.56%.  $J_{sc}$  is a reflection of accumulative electron density injected from excited state of dye to CB of TiO<sub>2</sub>, whereas the low excitation efficiency and photodegradation of dye molecules on TiO<sub>2</sub> nanocrystallites have been tremendous obstacles for current loss. Owing to the compensation effect of TiO<sub>2</sub>/SiO<sub>2</sub> nanocrystallines and enhancement of  $E_g$  of SiO<sub>2</sub> doped TiO<sub>2</sub>, the excitation efficiency and photostability of dye molecules can be

significantly improved, giving an enhanced  $J_{sc}$  in their DSSC devices. From a small standard deviation ( $\pm 5\%$ ), as shown in supporting information Fig. S1, we infer that the DSSCs with promising photovoltaic performances and high reproducibility can be realized using the method reported here.

From the dark  $J-V$  curves in Fig. 7b, one can see that the DSSC from  $\text{TiO}_2/\text{SiO}_2$ -(ii) anode shows the smallest dark current density at the same voltage. The dark current density in DSSC device is attributed to the triiodides combination with electrons on CB of  $\text{TiO}_2$  at the  $\text{TiO}_2$ /electrolyte interface.<sup>31</sup> The smaller dark current density indicates that the reduction of triiodides on the  $\text{TiO}_2$ /electrolyte interface is retarded. This is another factor for the elevated  $J_{sc}$  for  $\text{TiO}_2/\text{SiO}_2$ -(ii) anode based DSSC.

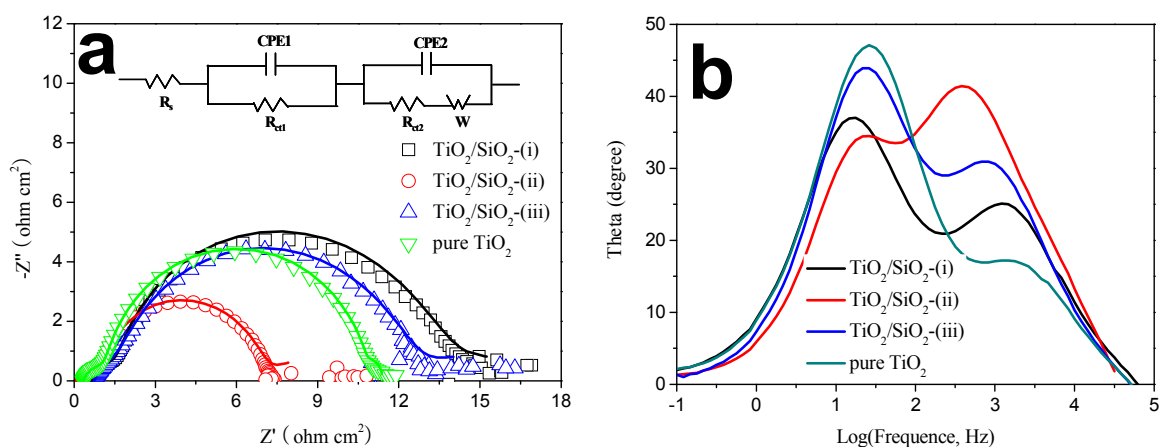


**Fig. 8** EIS spectra of the DSSCs from varied nanocrystallite anodes. The inset gives the equivalent circuit used to fit the impedance data. (a) Nyquist plot, (b) Bode phase plot.

**Table 3** Parameters of lifetime of electrons and the equivalent circuit obtained by fitting EIS of the DSSCs using a Z-view software.  $\tau$ : lifetime.

Parameters	$\text{TiO}_2/\text{SiO}_2$ -(i)	$\text{TiO}_2/\text{SiO}_2$ -(ii)	$\text{TiO}_2/\text{SiO}_2$ -(iii)	pure $\text{TiO}_2$
$R_s$ ( $\Omega \text{ cm}^2$ )	0.89	0.73	0.97	0.95
$R_{ct2}$ ( $\Omega \text{ cm}^2$ )	5.33	3.46	9.09	9.32
$W$ ( $\Omega \text{ cm}^2$ )	18.72	6.84	18.18	19.06
$\tau$ ( $\mu\text{s}$ )	124.2	399.7	214.9	105.1

Fig. 8a shows the impedance spectra for the DSSCs, giving two semicircles which are assigned to electrochemical reaction at CE (a smaller one in high frequency region) and charge transfer at the  $\text{TiO}_2|\text{dye}|$ electrolyte (a larger one in low frequency region). An equivalent circuit (see the inset of Fig. 8a) is used to fit the Nyquist plots to estimate the electron transport parameters, such as sheet resistance ( $R_s$ ), charge-transfer resistance at CE/electrolyte ( $R_{ct1}$ ), charge-transfer resistance at the  $\text{TiO}_2/\text{dye}/$ electrolyte interface ( $R_{ct2}$ ), and Nernst diffusion impedance corresponding to the diffusion resistance of  $\text{I}^-/\text{I}_3^-$  redox species ( $W$ ). CPE1 and CPE2 are constant phase elements. It is found that the  $R_{ct2}$  of  $\text{TiO}_2/\text{SiO}_2$ -(ii) anode based DSSC is the smallest in comparison with other devices. The results demonstrate that the photogenerated electrons can be rapidly transferred to CB of  $\text{TiO}_2$  and the excited dyes are easily recovered by iodide ions. Moreover, the smallest  $W$  value suggests that the  $\text{I}^-/\text{I}_3^-$  redox couples have a high diffusion kinetics within  $\text{TiO}_2/\text{SiO}_2$ -(ii) anode.

$$\tau = 1 / 2\pi f_p \quad (5)$$

Finally, the lifetimes of electrons on various anodes are determined according to equation (4),<sup>32</sup> where  $f_p$  is second peak frequency (Fig. 8b), giving a lifetime of 124.2  $\mu\text{s}$  for  $\text{TiO}_2/\text{SiO}_2$ -(i), 399.7  $\mu\text{s}$  for  $\text{TiO}_2/\text{SiO}_2$ -(ii), 214.9  $\mu\text{s}$  for  $\text{TiO}_2/\text{SiO}_2$ -(iii), and 105.1  $\mu\text{s}$  for pure  $\text{TiO}_2$ . The enhanced electron lifetime in  $\text{TiO}_2/\text{SiO}_2$  based DSSCs can be attributed to the elevated formation of connected channels by  $\text{TiO}_2$  and enhanced electron density.

#### 4. Conclusions

In summary, we have demonstrated that the combination of  $\text{TiO}_2$  with  $\text{SiO}_2$  is an effective strategy for enhancing dye illumination and excitation, and increasing dye photostability. Due to the light interference reflected from  $\text{TiO}_2/\text{SiO}_2$  and  $\text{SiO}_2/\text{air}$  (electrolyte) interfaces, more active sites for dye adsorption and high electron lifetime, the DSSC from  $\text{TiO}_2/\text{SiO}_2$ -(ii) nanocrystallite provides an

impressive power conversion efficiency of 8.56% in comparison with that of 7.06% from pure TiO<sub>2</sub> anode based device. The research presented here is far from being optimized but these profound advantages along with low-cost synthesis and scalable materials promise the new nanocrystallites to be strong candidates in robust DSSCs.

## Acknowledgements

The authors would like to acknowledge financial supports from National Natural Science Foundation of China (U1037604), Shandong Province Outstanding Youth Scientist Foundation Plan (BS2013CL015), Shandong Provincial Natural Science Foundation (ZR2011BQ017), and Research Project for the Application Foundation in Qingdao (13-4-198-jch).

## References

- 1 P. Krogstrup, H. I. Jorgensen, M. Heiss, O. Demichel, J. V. Holm, M. Aagesen, et al, *Nat. Photonics*, 2013, **7**, 306–310.
- 2 J. Oh, H. C. Yuan and H. M. Branz, *Nat. Nanotechnol.*, 2012, **7**, 743–748.
- 3 Y. Chiba, A. Islam, Y. Watanabe, R. Komiya, N. Koide and L. Han, *Jpn. J. Appl. Phys.*, 2006, **45**, L638–L640.
- 4 X. X. Chen, Q. W. Tang, B. L. He, L. Lin and L. M. Yu, *Angew. Chem. Int. Ed.*, 2014, **53**, 10799–10803
- 5 Y. Y. Duan, Q. W. Tang, J. Liu, B. L. He and L. M. Yu, *Angew. Chem. Int. Ed.*, 2014, **53**, 14569–14574
- 6 T. G. Deepak, G. S. Anjusree, S. Thomas, T. A. Arun, S. V. Nair and A. S. Nair, *RSC Adv.*, 2014, **4**, 17615–17638.

- 7 Q. W. Tang, H. Y. Cai, S. S. Yuan and X. Wang, *J. Mater. Chem. A*, 2013, **1**, 317–323.
- 8 K. Ladomenou, T. N. Kitsopoulos, G. D. Sharma and A. G. Coutsolels, *RSC Adv.*, 2014, **4**, 21379–21404.
- 9 B. O'Regan and M. Grätzel, *Nature*, 1991, **353**, 737–740.
- 10 A. Yella, H. W. Lee, H. N. Tsao, C. Yi, A. K. Chandiran, M. K. Nazeeruddin, et al, *Science*, 2011, **334**, 629–634.
- 11 S. S. Yuan, Q. W. Tang, B. L. He, L. Men and H. Y. Chen, *Electrochim. Acta*, 2014, **125**, 646–651.
- 12 H. S. Jung and J. K. Lee, *J. Phys. Chem. Lett.*, 2013, **4**, 1682–1693.
- 13 X. L. He, G. J. Yang, C. J. Li, C. X. Li and S. Q. Fan, *J. Power Sources*, 2014, **251**, 122–129.
- 14 J. H. Wu, Y. Li, Q. W. Tang, G. T. Yue, J. M. Lin, M. L. Huang, et al, *Sci. Rep.*, 2014, **4**, 4028.
- 15 Z. Weng, H. Guo, X. Liu, S. Wu, K. W. K. Yeung and P. K. Chu, *RSC Adv.*, 2013, **3**, 24758–24775.
- 16 L. Lin, Y. C. Yang, L. Men, X. Wang, D. N. He, Y. C. Chai, et al, *Nanoscale*, 2013, **5**, 588–593.
- 17 K. M. Reddy, S. V. Manorama and A. R. Reddy, *Mater. Chem. Phys.*, 2002, **78**, 239–245.
- 18 L. Lin, Y. Yang, L. Men, X. Wang, D. He, Y. Chai, B. Zhao, S. Ghoshroy and Q. W. Tang, *Nanoscale*, 2013, **5**, 588–593.
- 19 L. Lin, Y. Chai, Y. Yang, X. Wang, D. He, Q. W. Tang and S. Ghoshroy, *Int. J. Hydrogen Energy*, 2013, **38**, 2634–2640.
- 20 H. Y. Cai, X. X. Chen, Q. H. Li, B. L. He and Q. W. Tang, *Appl. Surf. Sci.*, 2013, **284**,

- 837-842.
- 21 Q. H. Zhang, L. Gao and J. K. Guo, *Appl. Catal. B-Environ.*, 2000, **26**, 207–215.
- 22 L. Q. Jing, X. J. Sun, B. F. Xin, B. Q. Wang, W. M. Cai and H. G. Fu, *J. Solid State Chem.*, 2004, **177**, 3375-3382.
- 23 Y. H. Zhang, H. X. Zhang, Y. X. Xu and Y. G. Wang, *J. Mater. Chem.*, 2003, **13**, 2261–2265.
- 24 C. H. Yang, Z. Q. Ma, F. Li, B. He, J. H. Yuan and Z. H. Zhang, *Acta Phys-Chim. Sin.*, 2010, **26**, 1349–1354.
- 25 I. Cacciotti, A. Bianco, G. Pezzotti and G. Gusmano, *Chem. Eng. J.*, 2011, **166**, 751–764.
- 26 S. Cheng, X. Liu, S. Yun, H. Luo and Y. Gao, *Ceram. Int.*, 2014, **40**, 13781-13786.
- 27 Y. Li, X. Ge, X. Pang, X. Yu, X. Zhen, L. Geng and Y. Wang, *Mater. Lett.*, 2015, **152**, 170-172.
- 28 T. Trupke, P. Würfel and I. Uhlendorf, *J. Phys. Chem. B*, 2000, **104**, 11484–11488.
- 29 I. Gonzalez–Valls, Y. Yu, B. Ballesteros, J. Oro and M. Lira–Cantu, *J. Power Sources*, 2011, **196**, 6609–6621.
- 30 X. Z. Guo, Y. H. Luo, C. H. Li, D. Qin, D. M. Li and Q. B. Meng, *Curr. Appl. Phys.*, 2012, **12**, e54–e58.
- 31 Z. Y. Tang, J. H. Wu, M. Zheng, J. H. Huo and Z. Lan, *Nano Energy*, 2013, **2**, 622–627.
- 32 T. Hoshikawa, T. Ikebe, R. Kikuchi and K. Eguchi, *Electrochim. Acta*, 2006, **51**, 5286–5294.

